JOURNAL OF MATERIALS SCIENCE 25 (1990) 1231–1236

Corrosion of Si_3N_4 and sialons in V_2O_5 melts

T. SATO, S. TERAUCHI, T. ENDO, M. SHIMADA
Department of Molecular Chemistry and Engineering, Faculty of Engineering, Tohoku University, Sendai 980, Japan

Si_3N_4 based ceramics such as hot isostatically pressed Si_3N_4, hot pressed Si_3N_4, hot pressed sialons containing 0, 30, 60 and 100% of α phase were corroded by V_2O_5 melts at 700 to 1000° C. These Si_3N_4-based ceramics were oxidized to SiO_2 and dissolved into V_2O_5 melts. The surface chemical reaction controlled shrinking core model adequately described the relationship between the weight loss of the specimen and time for the corrosion reactions in V_2O_5 melts, and the apparent activation energies were 69 to 112 kJ mol^{-1}. β phase Si_3N_4 and sialon showed higher corrosion resistance than α phase sialons, but no clear relationship between the corrosion rate and the content of additives was found. The specimens corroded by V_2O_5 melts showed no significant degradation in the fracture strength up to 30 wt% of weight loss.

1. Introduction

Since non-oxide ceramics such as silicon nitride and silicon carbide can retain excellent fracture strength at high temperature and are remarkably resistant to thermal shock fracture and oxidizing combustion, they are considered as good candidates for structural application at high temperature such as hot gas turbines, heat exchangers and insulating walls. However, these ceramics are inherently unstable in an oxidizing atmosphere. Therefore, it is essential to investigate the effect of hot corrosion attack on the mechanical properties of these non-oxide ceramics which generally form an SiO_2 layer on the surface in an oxidizing atmosphere. Oxidation behaviour extensively depended on the characteristics of the SiO_2 protective layer. McKee and Chatterji [1], Mayer and Riley [2], Brook *et al.* [3] and Erdoes and Altorfer [4] have investigated the corrosion behaviour of silicon carbide and silicon nitride in a variety of molten salt/gas environments. They reported that the oxygen potential at the surface of silicon carbide and silicon nitride was a critical parameter for the "active" and "passive" oxidation in gaseous and molten salt environments. Becher [5] studied the fracture strength degradation of silicon carbide and silicon nitride ceramics resulting from the exposure to coal slags at high temperature, and reported that the strength degradation greatly depended on the chemical constitution of the slags, i.e., fracture strength of hot-pressed Si_3N_4 exposed in an acid slag decreased up to 65%, but a basic slag caused remarkably little strength degradation in spite of the large corrosion rate. Recently, it was reported that alkali sulphate and alkali carbonate melts could oxidize silicon nitride and silicon carbide to liquid alkali silicate and cause significant strength degradation [6–11]. In general, combustion gas contains a corrosive element of vanadium together with sodium, potassium, sulphur, etc., thereby V_2O_5 and various vanadates sometimes condense on the wall. Since V_2O_5 possesses strong oxidation potential and high solubility of SiO_2, it was suspected to cause severe strength degradation of silicon nitride based ceramics by corrosion, but no systematic study for the corrosion behaviour of silicon nitride ceramics by V_2O_5 melts has yet been reported. In the present work, a series of corrosive reaction experiments was conducted to obtain more detailed information on the corrosion behaviour of silicon nitride based ceramics in V_2O_5 melts.

2. Experimental procedure

Hot isostatically pressed Si_3N_4 without additives, hot pressed Si_3N_4 and hot pressed sialons containing 0, 30, 60 and 100% of α phase, denoted as HIP-Si_3N_4,

TABLE I Characteristics of the samples

Sample	Phase (%)		Chemical compositions (at. %)					K_{IC} (MPa m$^{1/2}$)	σ_{3b} (MPa)
	α	β	Si	N	Y	Al	O		
HIP-Si_3N_4	0	100	42.9	57.1	0	0	0	3.98	753
HP-Si_3N_4	0	100	41.2	54.8	0.86	0.76	2.44	5.29	870
Sialon-0	0	100	38.5	52.4	0.86	3.51	4.77	3.60	935
Sialon-30	30	70	41.2	56.4	0.34	1.58	0.51	4.31	717
Sialon-60	60	40	37.6	55.0	1.06	4.77	1.59	5.01	702
Sialon-100	100	0	34.2	53.5	1.74	7.94	2.65	4.94	552

α: α-Si_3N_4 phase, β: β-Si_3N_4 phase

0022–2461/90 $03.00 + .12

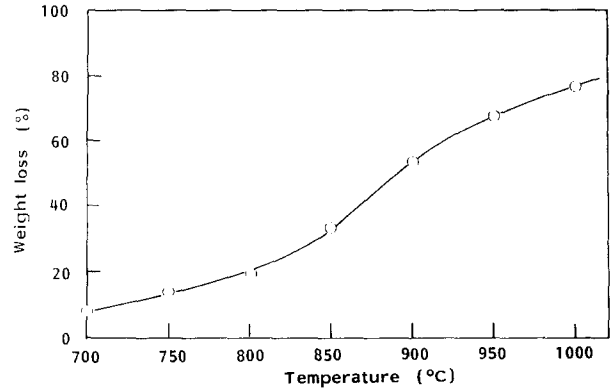

Figure 1 Degree of weight loss of HP-Si_3N_4 corroded in V_2O_5 melts at various temperatures.

HP-Si_3N_4, Sialon-0, Sialon-30, Sialon-60 and Sialon-100 were used as corrosion samples. The characteristics of these ceramics are summarized in Table I. HIP-Si_3N_4, HP-Si_3N_4 and Sialon-0 were β-Si_3N_4 phase and Sialon-100 was α-Si_3N_4 phase. On the other hand, Sialon-30 and Sialon-60 were mixtures of α-Si_3N_4 and β-Si_3N_4 phases. The amounts of α-Si_3N_4 phase were determined by Gazzara's method [12].

All samples were cut into rectangular coupons, 4 × 5 × 15 mm. In each experiment, a weighed sample and powdered reagent grade V_2O_5 were put into a platinum tube, 16 mm in diameter and 170 mm long, then placed in an electric furnace regulated at the desired temperature. The corrosion reaction was carried out in V_2O_5 melts exposed to air in order to prevent the precipitation of the reduced vanadium oxide such as VO_2, V_2O_3, etc. The initial molar ratio of V_2O_5 : Si_3N_4 was 40. After maintaining the desired temperature and time, the tube was removed from the electric furnace and cooled quickly to room temperature. The samples were washed with 1 M HCl solution and hot water, dried, and weighed. The crystalline phase and microstructure of the samples were examined by X-ray diffraction analysis, infrared spectroscopy and scanning electron microscopy. The fracture strength of the sample was determined by a three-point bending test with a cross-head speed of 0.5 mm min^{-1} and span length of 10 mm.

3. Results and discussion

The degree of weight loss of HP-Si_3N_4 corroded in V_2O_5 melts at various temperatures for 3 h is shown in Fig. 1. The sample showed no noticeable weight change in air below 1000° C, but showed significant weight loss above 700° C in V_2O_5 melts, and the corrosion rate increased with rising temperature. The specimens shrunk isotropically by corrosion. No reaction product was detected by X-ray diffraction analysis and scanning electron microscopy on the surface of the corroded sample. Therefore, Si_3N_4 seemed to dissolve into the V_2O_5 melt.

In order to determine the reaction product, Si_3N_4 powders were reacted with V_2O_5 melt by the molar ratio of V_2O_5 : Si_3N_4 of 0.5 at 900° C for 5 hr. An infrared spectrum of the reaction product is shown in Fig. 2 together with those of Si_3N_4 and V_2O_5. The absorption peaks at 470, 800 and 1100 cm^{-1} corresponding to Si–O stretching were observed. On the other hand, no diffraction peak corresponding to reaction product was observed by X-ray diffraction analysis. These results indicated that Si_3N_4 was oxidized to the amorphous SiO_2 and dissolved into V_2O_5 melt as expressed by Equations 1 and 2.

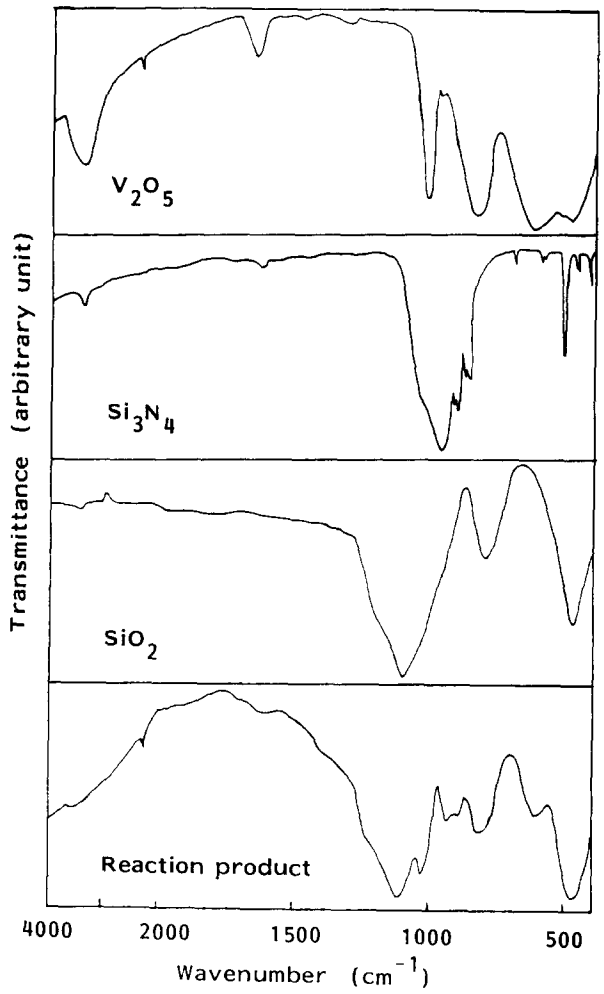

Figure 2 Infrared spectra of the reaction product, SiO_2 glass, Si_3N_4 and V_2O_5.

$$Si_3N_4 + 3V_2O_5 = 3SiO_2 + 3V_2O_3 + 2N_2 \quad (1)$$

$$V_2O_3 + O_2 = V_2O_5 \quad (2)$$

HP-Si_3N_4 was reacted with various amounts of V_2O_5 melts at 1000° C. The time dependence of the fractional weight loss, α, of the specimen is shown in Fig. 3 as a function of molar ratio of V_2O_5 : Si_3N_4. In the heterogeneous reaction systems such as solid and liquid phases, when the shrinking core model is applied and the surface chemical reaction process is rate-limiting, the relation between α and time, t, is expressed by Equation 3.

$$1 - (1 - \alpha)^{1/3} = kt r_0^{-1} \quad (3)$$

where r_0 is the radius of the sample and k is the rate constant. Since the specimens used in the present study are rectangular coupons, r_0 is defined as $3abc/2(ab + bc + ca)$, where a is the specimen width, b is the specimen thickness and c is the specimen length, respectively. The plots of $1 - (1 - \alpha)^{1/3}$ against time are also shown in Fig. 3. As seen in Fig. 3, the corrosion data for the reaction of V_2O_5 : Si_3N_4 with molar ratio of 40 is adequately described by Equation 3, but the

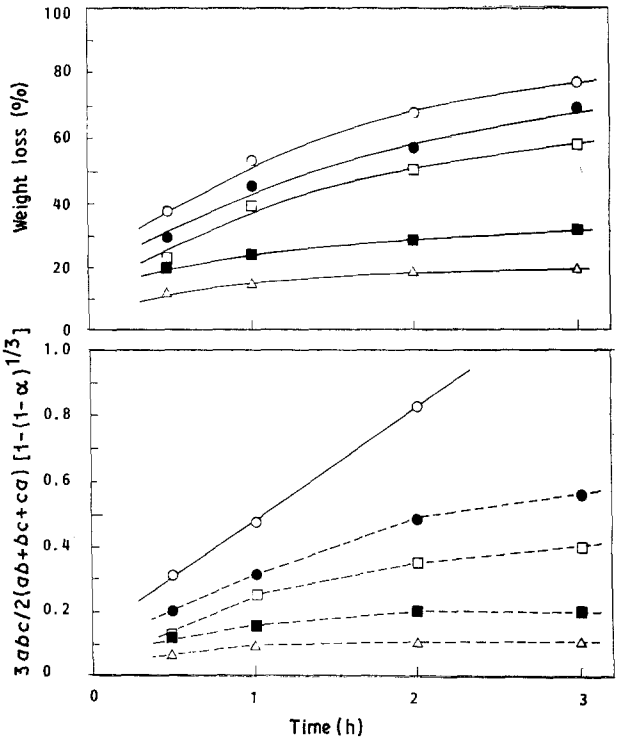

Figure 3 Time dependence of the weight loss of HP-Si_3N_4 corroded in various amounts of V_2O_5 melts. Molar ratio V_2O_5 : Si_3O_4 — ○, 40; ●, 30; □, 20; ■, 10; △, 5.

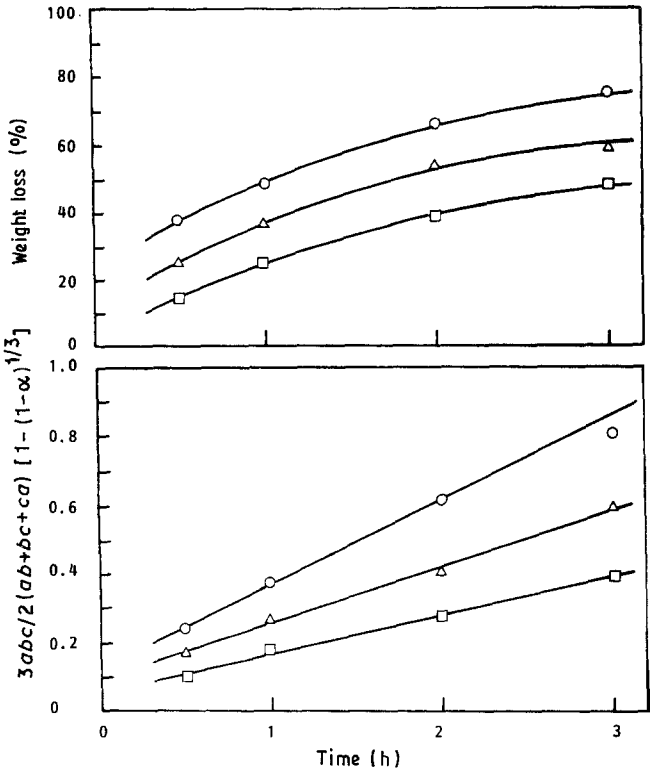

Figure 5 Plots of $1-(1-\alpha)^{1/3}$ against time for the corrosion reaction of HP-Si_3N_4 in V_2O_5 melts at 900 to 1000° C. ○, 1000° C; △, 950° C; □, 900° C.

values of $1-(1-\alpha)^{1/3}$ did not increase proportionately with time for the reaction of V_2O_5 : Si_3N_4 with molar ratio below 30. These results indicated that a protective layer of reaction product was formed on the surface of Si_3N_4 in the reaction when the molar ratio of V_2O_5 : Si_3N_4 was below 30. The phase diagram of the SiO_2–V_2O_5 system [13] is shown in Fig. 4. It was seen that about 7.5 mol % of SiO_2 can dissolve into V_2O_5 at 1000° C. Therefore, SiO_2 formed by corrosion could entirely dissolve into V_2O_5 melt, when the V_2O_5 : Si_3N_4 molar ratio was more than 40. On the other hand, when the molar ratio was less than 30, SiO_2 should precipitate on the surface, and inhibit the corrosion reaction.

The plots of $1-(1-\alpha)^{1/3}$ against time for the

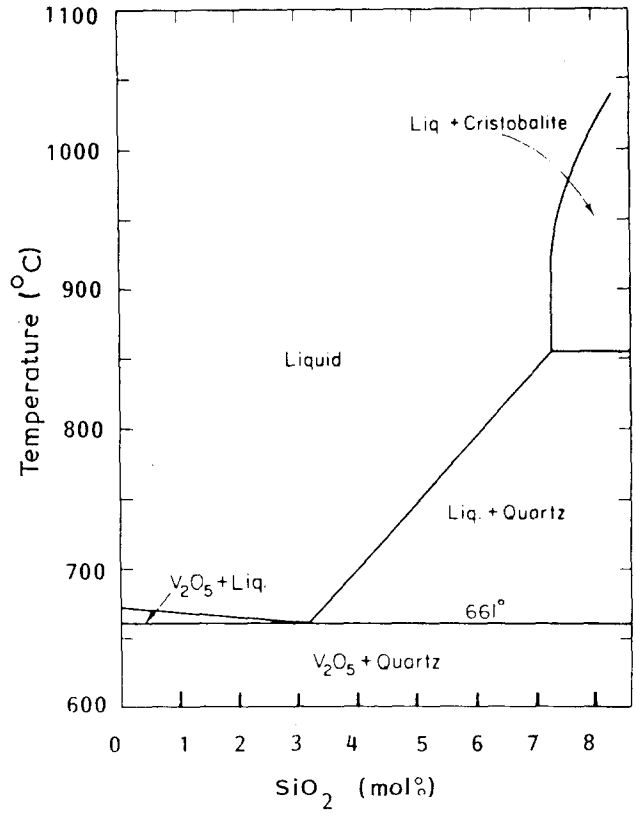

Figure 4 Phase diagram of SiO_2–V_2O_5 system [13].

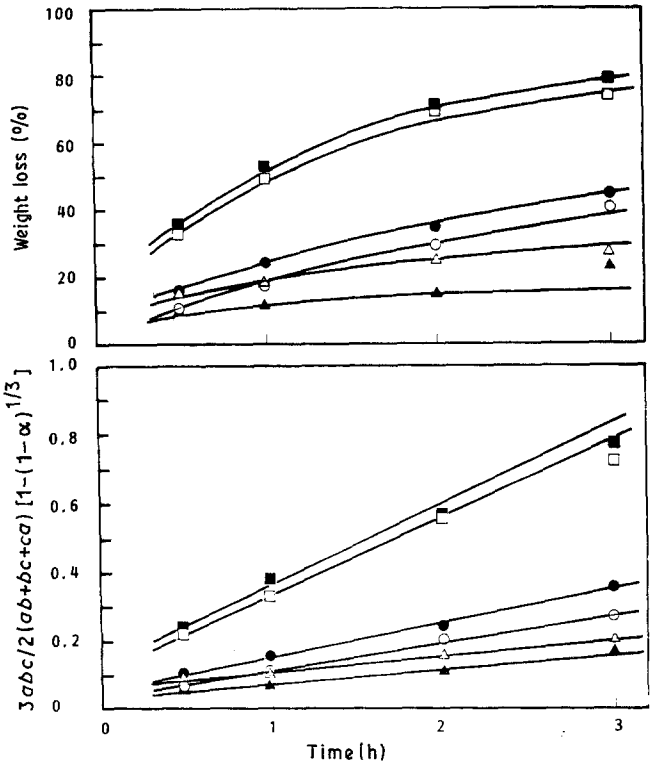

Figure 6 Time dependence of the weight loss for HIP-Si_3N_4 in V_2O_5 melts coexisting with various oxides at 900° C. ○, V_2O_5; ● V_2O_5–Al_2O_3; △, V_2O_5–CaO; ▲, V_2O_5–Fe_2O_3; □, V_2O_5–K_2O; ■, V_2O_5–Na_2O.

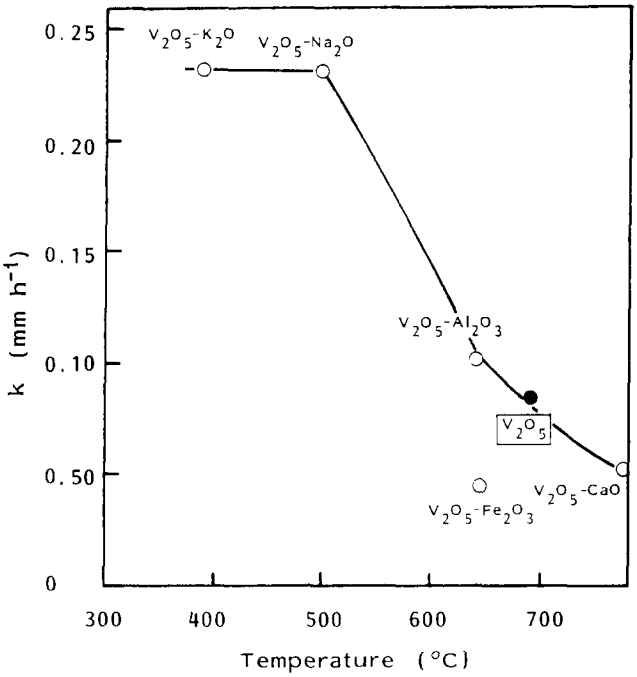

Figure 7 The relationship between the corrosion rate constant and the melting temperature of the melts.

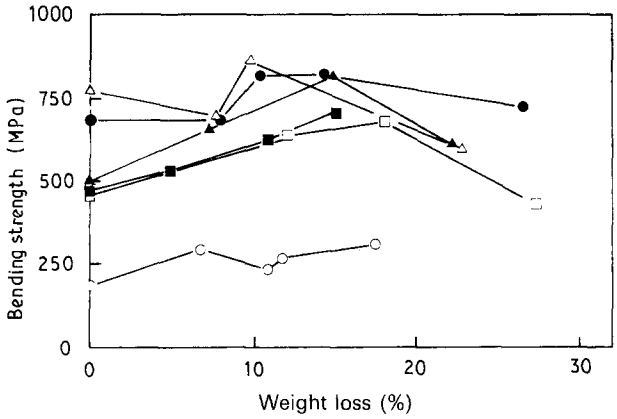

Figure 8 Three-point bending strength of various Si_3N_4 and sialons corroded in V_2O_5 melts at 900° C for various times. ○, HIP-Si_3N_4; ●, H; □, Sialon-0; ■, Sialon-30; △, Sialon-60; ▲, Sialon-100.

corrosion reaction of HP-Si_3N_4 in V_2O_5 melts at 900 to 1000° C are shown in Fig. 5. From the slope of the straight lines, the rate constant, k, was determined. Similar experiments were carried out for all samples. The rate constants and the activation energies determined from the slope of the Arrhenius plots are summarized in Table II together with the total contents of aluminium and yttrium in the samples. The apparent activation energies were 69 to 112 kJ mol^{-1}. It seemed that the corrosion rate of β phase Si_3N_4 and sialon was smaller than that of α phase sialons. In the previous paper [11], it was reported that the corrosion resistance of Si_3N_4 and sialons in alkali sulphate and alkali carbonate melts increased with increasing content of additives such as Al_2O_3 and Y_2O_3. However, no clear relationship between the corrosion rate and the content of additives was found for the corrosion reaction of Si_3N_4 and sialons in V_2O_5 melts.

The corrosion behaviour of HIP-Si_3N_4 in V_2O_5 melts coexisting with various oxides was investigated at 900° C, and the results are summarized in Fig. 6, where the molar ratios of V_2O_5 : Si_3N_4 and oxide additives: Si_3N_4 were 30 and 15, respectively. It was found that addition of Na_2O and K_2O into V_2O_5 greatly promoted the corrosion reaction, but that of CaO and Fe_2O_3 decreased the corrosion rate. It was generally found that the corrosion of silicon nitride in the melts such as alkali sulphate, alkali carbonate [9] and coal slags [5] was promoted by decreasing the melting temperature and increasing the basicity of the melts. The relationship between the corrosion rate constant and the melting temperature of the melts is shown in Fig. 7. It was seen that the corrosion rate increased by decreasing the melting temperature of the melts, but no good relationship between the corrosion rate and basicity of the melts was observed.

Three-point bending strengths, σ_{3b}, of Si_3N_4 and sialons corroded in V_2O_5 melts at 900° C for various times are determined according to Equation 4, and the results are shown in Fig. 8 as

$$\sigma_{3b} = 3PL/2ab^2 \quad (4)$$

a function of the degree of weight loss of the sample, where P is the applied load and L is the span length. No noticeable degradation of the fracture strength was observed up to about 30% weight loss. These results indicated that the large pits as the fracture origin were not formed on the surface of the sample by the corrosion reaction where silicon nitride based ceramics significantly dissolved into V_2O_5 melts. The scanning electron micrographs of the surface and the cross section of HP-Si_3N_4 before corrosion and after corrosion at 900° C with up to 26% weight loss are shown in Fig. 9. The surface was etched by V_2O_5 melt and the needle like grains of Si_3N_4 were observed on the surface of the corroded sample. However, as expected, no large pit was observed in the scanning electron micrograph of the cross-section of the corroded sample. Since corrosion of silicon nitride and sialons proceeded isotropically and the fracture strength was almost constant, Equation 4 can be

TABLE II Rate constants and apparent activation energies of the corrosion of various silicon nitrides and sialons in V_2O_5 melts

Sample	Content of Al + Y (at. %)	Rate constant (mm h^{-1})			Activation energy (kJ mol^{-1})
		900° C	950° C	1000° C	
HIP-Si_3N_4	0	0.15	0.19	0.34	101
HP-Si_3N_4	4.06	0.11	0.17	0.25	97
Sialon-0	9.14	0.17	0.23	0.32	79
Sialon-30	2.43	0.18	0.23	0.32	69
Sialon-60	7.42	0.17	0.28	0.42	112
Sialon-100	12.3	0.22	0.29	0.38	69

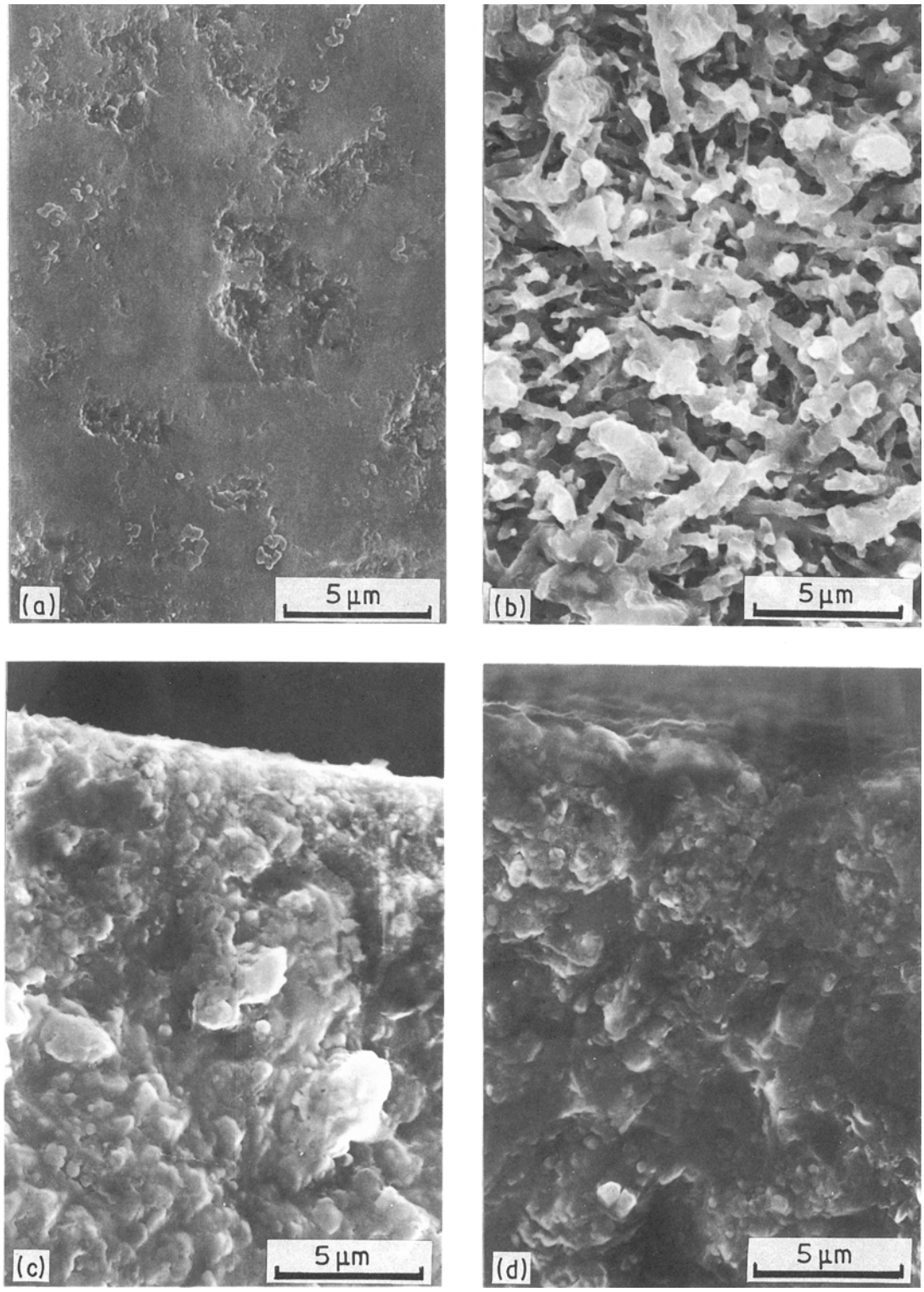

Figure 9 Scanning electron micrographs of the surface and the cross-section of HP-Si_3N_4 before corrosion and after corrosion in V_2O_5 melt at 900° C up to 26% weight loss. (a) Surface before corrosion; (b) Surface after corrosion; (c) Cross-section before corrosion; (d) Cross-section after corrosion.

modified as Equation 5.

$$P_t = 2ab^2(1 - x)^3/3\sigma_{3b}L = 2ab^2(1 - \alpha)/3\sigma_{3b}L = P_0(1 - \alpha) \quad (5)$$

where P_0 and P_t are the fracture loads of the original sample and corroded sample, respectively, x is the fractional shrinkage of the sample. Thus, the fracture load of the corroded sample is proportional to the volume of the sample remaining. Therefore, it might be possible to predict the time to rupture for the corroded sample under an applied load, P_t, by using the present kinetic data for corrosion reaction.

4. Conclusions

From the present experimental results, the following conclusions may be drawn.

1. Si_3N_4-based ceramics were oxidized and dissolved into V_2O_5 melt.

2. The surface chemical reaction controlled

shrinking core model could be applied to describe the relationship between the degree of corrosion and the reaction time for the corrosion of Si_3N_4-based ceramics in V_2O_5 melts.

3. The apparent activation energies for the corrosion of Si_3N_4-based ceramics in V_2O_5 melts were 69 to 112 kJ mol^{-1}.

4. The corrosion of Si_3N_4-based ceramics in V_2O_5 melts was promoted by coexisting compounds and decreasing the melting temperature of the melt.

5. Corrosion resulted in the shrinkage of the sample, but no noticeable degradation in the fracture strength occurred up to 30% weight loss.

Acknowledgement

This work has been supported in part by a grant-in-aid for Energy Research of the Ministry of Education.

References

1. D. W. MCKEE and D. CHATTERJI, *J. Amer. Ceram. Soc.* **59** (1976) 441.
2. M. I. MAYER and F. L. RILEY, *J. Mater. Sci.* **13** (1978) 1319.
3. S. BROOK, J. M. FERGUSON, D. B. MEADOWCROFT and C. G. STEAVENS, in "Materials and Coatings to Resist High Temperature Corrosion", edited by D. R. Holmes and A. Rahemel (Applied Science, London, 1977) p. 121.
4. E. ERDOES and H. ALTORFER, in "Materials and Coatings to Resist High Temperature Corrosion" edited by D. R. Holmes and A. Rahemel (Applied Science, London, 1977) p. 161.
5. P. F. BECHER, *J. Mater. Sci.* **19** (1984) 2805.
6. R. E. TRESSLER, M. D. MEYSER and T. YONUSHONIS, *J. Amer. Ceram. Soc.* **59** (1976) 278.
7. W. C. BOURNE and R. E. TRESSLER, *Amer. Ceram. Soc. Bull.* **59** (1980) 443.
8. M. K. FERBER and V. J. TENNERY, *ibid.* **62** (1983) 236.
9. T. SATO, Y. KANNO, T. ENDO and M. SHIMADA, *Adv. Ceram. Mater.* **2** (1987) 228.
10. J. L. SMIALEK and N. S. JACOBSON, *J. Amer. Ceram. Soc.* **69** (1986) 741.
11. T. SATO, Y. KOIKE, T. ENDO and M. SHIMADA, *J. Mater. Sci.* **23** (1988) 1405.
12. C. P. GAZZARA and D. R. MEISSIER, *Amer. Ceram. Soc. Bull.* **56** (1977) 777.
13. N. C. GRAVETTE, D. BARHAM and L. R. BARRETT, *Trans. Brit. Ceram. Soc.*, **65** (1966) 205.

Received 14 November 1988
and accepted 26 April 1989